DIFFUSION OF NEODYMIUM IN ORTHOPYROXENE: EXPERIMENT, THEORY AND APPLICATIONS

by

Jennifer L. Sano

A Thesis Submitted to the Faculty of the

DEPARTMENT OF GEOSCIENCES

In Partial Fulfillment of the Requirements
for the Degree of

MASTER OF SCIENCE

In the Graduate College
THE UNIVERSITY OF ARIZONA
2007

STATEMENT BY THE AUTHOR

This thesis has been submitted in partial fulfillment of requirements for the Master of Science degree at The University of Arizona and is deposited in the Antevs Reading Room to be made available to borrowers, as are copies of regular theses and dissertations.

Brief quotations from this manuscript are allowable without special permission, provided that accurate acknowledgment of the source is made. Requests for permission for extended quotation from or reproduction of this manuscript in whole or in part may be granted by the Department of Geosciences when the proposed use of the material is in the interests of scholarship. In all other instances, however, permission must be obtained from the author.

_____ _____

(author's signature) *(date)*

APPROVAL BY RESEARCH COMMITTEE

As members of the Research Committee, we recommend that this thesis be accepted as fulfilling the research requirement for the degree of Master of Science.

_____ _____

Major Advisor *(type name)* *(signature)* *(date)*

_____ _____

(type name) *(signature)* *(date)*

_____ _____

(type name) *(signature)* *(date)*

Table of Contents

List of Illustrations

List of Tables

Abstract

We have determined the Arrhenius relation for neodymium (Nd) diffusion in orthopyroxene parallel to the b- axial direction as a function of temperature at 1 bar pressure and at *f*(O2) corresponding to that of the wüstite-magnetite buffer. Experiments were also carried out to determine Nd diffusion parallel to the a- and b-axial directions, and thus to develop an approximate idea of the extent of diffusion anisotropy of Nd in orthopyroxene, in which the three crystallographic axes define the directions of the three principal diffusion axes. It was found that D(//c) > D(//a) > D(//b) with around a factor of 10 change of diffusivity between D(//c) and D(//b). The difference between the diffusivities parallel to b and a axes is relatively small. From these data, we calculate Nd diffusion normal to the (210) plane of orthopyroxene in order compare our data with those of Cherniak and Liang (2006), who have determined Nd diffusion in orthopyroxene in the same direction. We find that our diffusion data yields a value of Nd diffusion normal to 210 plane at 1 bar, 1150 °C that is about a factor three greater than what follows from the Arrhenius relation given by Cherniak and Liang for REE diffusion in orthopyroxene. These authors claimed that the REE diffusion in orthopyroxene is independent of the nature of the trivalent REE, and thus combined all data to produce a single Arrhenius relation for all REE. However, our data for Nd diffusion normal to (210) plane is in good agreement with the specific experimental data of Cherniak and Liang for Nd diffusion. Thus, their conclusion that trivalent REE diffusion in orthopyroxene is essentially independent of the nature or radius of the REE may be questionable.

We have used our diffusion data parallel to the b-axis to calculate the closure temperature of Sm-Nd decay system in orthopyroxene grains of plane sheet and spherical habit as function of initial temperature, cooling rate and grain size. The Nd diffusion data were also used to interpret the resetting of mineral age defined by an internal isochron involving orthopyroxene in the Morristown mesosiderite, and to the problem of inference of cooling rate of spinel-peridotite on the basis of REE zoning in orthopyroxene.

Chapter 1. Introduction

Knowledge of the distribution and migration of rare earth elements is a valuable tool that has been used for decades to learn about the origin and evolution of magma on the Earth, moon, Mars and meteorites. By understanding partitioning behavior, geochemists have been able to determine magma source regions and partial melting processes from the observed chondrite normalized REE patterns. However, to better understand the observed distributions, it is essential to understand the transport processes that influence the development of these patterns, an important component of which is intra-crystalline or volume diffusion. A significant amount of data is available for diffusion coefficients of REE in garnet and clinopyroxene that act as primary hosts of REE in the upper mantle of the Earth. But until recently, little data had been available for REE in orthopyroxene, an important mineral for both terrestrial and planetary samples. In many planetary samples, the mineral ages have been determined by Sm-Nd isochrons involving orthopyroxene, as this is an abundant mineral in meteorites. Interpretation of these Sm-Nd ages in terms of planetary processes requires an understanding of the Nd diffusion in orthopyroxene and its diffusion closure temperature that defines the temperature at which the Sm-Nd geochronological clock stars "ticking" during cooling of a sample.

This work presents initial results of ongoing experimental studies to determine Nd diffusion coefficients in orthopyroxene. We compare our findings with recently published data by Cherniak and Liang (2007), and discuss implications of the similarities and differences. These authors have, however, determined REE diffusion normal to (210)

plane and carried out very limited number of experiments for Nd diffusion in orthopyroxene. They concluded that the diffusivities of trivalent REE in orthopyroxene are very similar so that a single Arrhenius relation that is defined primarily by the data for Gd diffusion yields the diffusivity of all trivalent REE. However, a close examination of their data shows that Nd diffusion could be significantly faster than that defined by their all encompassing Arrhenius relation. In addition, they concluded on the basis of very limited experimental data that there is no significant diffusion anisotropy for Nd diffusion in orthopyroxene. This conclusion is rather surprising since orthopyroxene is an anisotropic mineral and significant diffusion anisotropy for Fe-Mg diffusion was predicted, on theoretical grounds, by Ganguly and Tazzoli (1994) and confirmed experimentally by Schwandt et al. (1995), and Cr diffusion in orthopyroxene was also found to be significantly anisotropic (Ganguly et al., 2007). Other anisotropic minerals such olivine (e.g. Buening and Buseck, 1973, Misener, 1974, Chakraborty, 1994, Ito and Ganguly, 2006) and melilite (Ito and Ganguly, 2005) also show significant anisotropy of diffusion of di- and tri-valent cations. The data presented here provides the Nd diffusion coefficient (D) in orthopyroxene parallel primarily to the b- axial direction as a function of temperature at 1 bar pressure and at f(O2) corresponding to the wüstite-magnetite buffer and limited Nd diffusion data parallel to the a- and c- axial directions. We also discuss the implications of these diffusion data for the closure temperature of the Sm-Nd decay system in orthopyroxene, resetting of Sm-Nd age of orthopyroxene in planetary samples and retrieval of cooling rate of spinel peridotite from Nd zoning profiles in orthopyroxene.

Chapter 2. Experimental Study

Material and sample preparation:

Gem-quality natural magnesium-rich (96 percent enstatite content) orthopyroxene crystals from Sri Lanka were used in this work. The composition of the material was determined by a Cameca SX50 electron microprobe. The chemical composition of a typical crystal is presented in Table 2.1.

Prior to preparation for diffusion experiments, crystals were oriented in a Bruker Apex X8 single crystal diffractometer. The X8 produces 3x3 orientation matrices of a crystal which are fixed to a pin and marked for cutting along a chosen orientation. These crystals were then cut into thin slices keeping them oriented so that the polished face would be normal to the desired axial direction for the diffusion experiment. The samples were polished stepwise down from 1- to 0.25-micron aluminum powder and finished to a mirror-polish by a combination of chemical and mechanical polishing using silica suspension. The last step was done to remove a thin disturbed layer that usually develops close to a crystal surface after the mechanical polishing.

Experimental procedure:

Each sample is pre-annealed at the chosen experimental temperature and oxygen fugacity for 24 to 36 hours. Pre-annealing is done to equilibrate the point defect concentrations to the experimental conditions and to repair any damage near the surface caused by the mechanical polishing during sample preparation. Then a thin layer of neodymium oxide (Nd_2O_3) was deposited on the annealed sample faces by thermal

Table 2.1					
Electron probe data (average of six analyses) of enstatite used in the diffusion study					
Oxide	**wt%**	**1σ**		**Atom proportion**	**1σ**
Na_2O	0.01	0.01	Na	0.00	0.00
SiO_2	57.46	0.20	Si	1.94	0.00
MgO	38.01	0.06	Mg	1.91	0.00
Al_2O_3	2.44	0.05	Al	0.10	0.00
CaO	0.15	1.05	Ca	0.01	0.00
MnO	0.02	0.01	Mn	0.00	0.00
FeO	1.80	0.06	Fe	0.05	0.00
TiO_2	0.03	0.03	Ti	0.00	0.00
CrO_3	0.01	0.00	Cr	0.00	0.00
			Cations	**4.01**	
Total	**99.93**		**Oxygen**	**6.00**	

Table 2.2						
Nd diffusion in enstatite at WM buffer and results from anneals						
Sample	**D**	**log (D)**	**1σ**	**Axial direction**	**T (°C)**	**Time (h)**
NdEna01	1.55E-17	-16.81	0.058	//a	1025	241
NdEnb01	4.79E-18	-17.32	0.184	//b	1025	241
NdEnc01	4.47E-17	-16.35	0.037	//c	1025	241
NdEnb02.1	1.38E-17	-16.86	0.074	//b	1063	96
NdEnb02.2	1.62E-17	-16.79	0.082	//b	1063	168
NdEnb02.3	1.17E-17	-16.93	0.048	//b	1063	240
NdEnb03	3.31E-17	-16.48	0.070	//b	1095	98.5
NdEna04	1.55E-16	-15.81	0.037	//a	1150	48
NdEnb04	6.46E-17	-16.19	0.049	//b	1150	48
NdEnc04	1.41E-16	-15.85	0.058	//c	1150	48

evaporation under very high vacuum conditions. All experiments were carried out in a vertical gas mixing furnace at controlled fO_2 condition that was imposed by computer controlled flowing mixture of CO and CO_2. The experimental conditions and calculated diffusion rates are summarized in Table 2.2.

Sample analysis:

After careful preparation and appropriate anneal time, as describe above, the samples were analyzed by depth-profiling, and the diffusion profiles and element concentrations were obtained in an ion microprobe in the Cameca ims-3f SIMS and -6f SIMS (Secondary Ion Mass Spectrometer) at the Arizona State University. In order to minimize electrostatic charge by the primary ion beam during SIMS analysis, a thin film of ^{197}Au was deposited on the sample surface. The Nd diffusion profiles were measured as the change in concentration of ^{144}Nd with depth. The non-diffusing species ^{30}Si, ^{44}Ca and ^{26}Mg were also measured simultaneously during the sputtering process in order to help determine the location of the thin film and crystal surfaces and to monitor the stability of the analyses. Previous studies have shown that the Nd thin film is located at half the Au peak intensity (e.g. Ito and Ganguly, 2006), and the crystal surface lies very close to the position of the ^{30}Si peak (Ganguly et al. 1998). Intensities for the non-diffusing species – Ca, Si and Mg – are not stable for the first four or five measurement cycles, as seen in Fig. 2.1, therefore, the count rates for the Nd diffusion for those cycles are not used in the modeling of Nd diffusion profiles. Data obtained from depth profiling of an annealed sample are shown in Fig. 2.2.

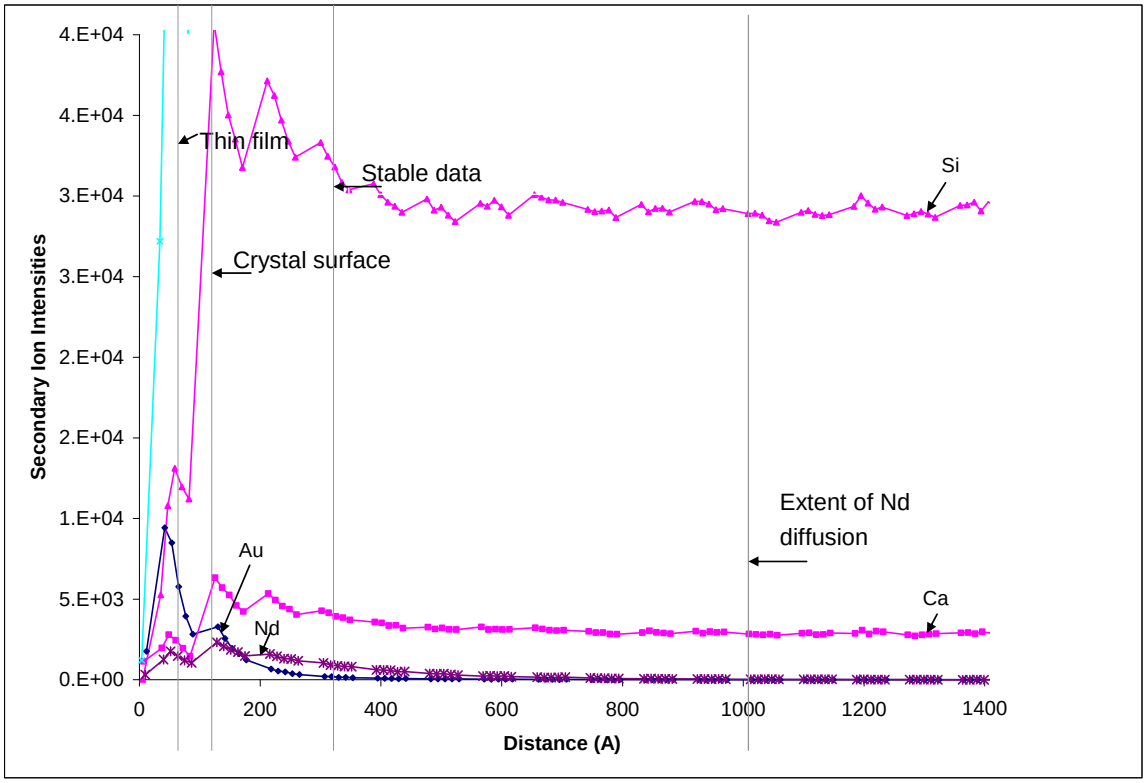

Figure 2.1: Secondary ion intensities of ^{144}Nd and the non-diffusing species ^{30}Si, ^{44}Ca and ^{26}Mg as measured by SIMS. The depth at which the thin film surface and crystal surface were determined to be, as well as where the stable data began and the depth coinciding with the extent of Nd diffusion are indicated by dark black lines. The thin film is determined to be at half the intensity of the Au peak and the sample surface is assumed to be between the thin film surface and the plateau intensity of non-diffusing species (e.g. Ito and Ganguly, 2006).

Statistical errors in D values were determined by considering the scatter of the normalized concentration data around the model fits and the effects of errors in the measurement of crater depths. Typically the contribution of error from the crater depth is negligible within ± 50 angstrom for a 1000 angstrom diffusion profile. The same is true for the contribution of error from choosing the depth at which the crystal surface occurs.

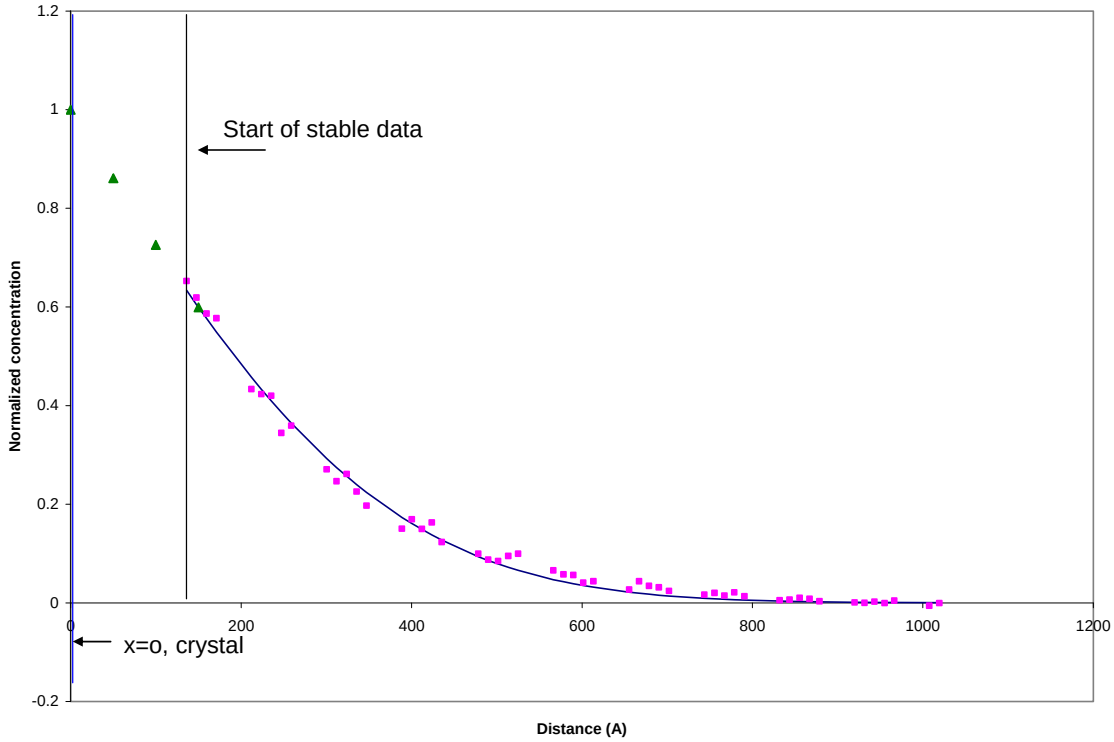

Fig. 2.2 A diffusion profile from an optimization program that finds the best fit to the experimental diffusion data according to the solution of the diffusion equation for a semi-infinite medium and a semi-infinite source. The experimental data (pink dots) are from a run at 1025 °C for diffusion parallel to the b-axial direction. The solid dark blue curve is the model fit. The green triangles are the values back calculated according to the diffusion equation to the crystal surface (thick blue line, x=0).

Chapter 3. Results and Discussion

Data analysis:

Once the proper surface location and diffusion profile length were determined, this information along with the experimental parameters were input into an optimization program (Tirone et al., 2005) which finds the best fit to the data according to the solution of the diffusion equation for diffusion in a semi-infinite medium that has uniform initial composition and a semi-infinite homogeneous source of the diffusing species. For these initial and boundary conditions, the solution of the diffusion equation is (Crank, 1975)

$$\frac{C_s - C(x,t)}{C_o - C_\infty} = erf\left(\frac{x}{2\sqrt{Dt}}\right) \qquad \text{Eq. 1}$$

where Cs is the concentration of the diffusing species at the surface of the mineral, C(x,t) is the concentration at distance x and time t, C_o is the fixed concentration at the surface, C_∞ is the concentration at a far enough distance where it has maintained its initial concentration, D is the diffusion coefficient, and t is time. Previous tracer diffusion studies using similar experimental procedures (Ito and Ganguly, 2004, 2006; Tirone et al., 2005) have shown that the solution for a semi-infinite source always yields the best fit to experimental data, as opposed to solving the diffusion equation using a depleting source.

Because diffusion coefficient is time independent, a time series analysis was conducted to test if the retrieved D value shows any dependence on time, in which case

the transport process could not be purely diffusion controlled. The experiment was run at 1065 °C for 96, 168 and 240 hours. The results, illustrated in Fig. 3.1, do not show any systematic dependence of D(Nd) on time.

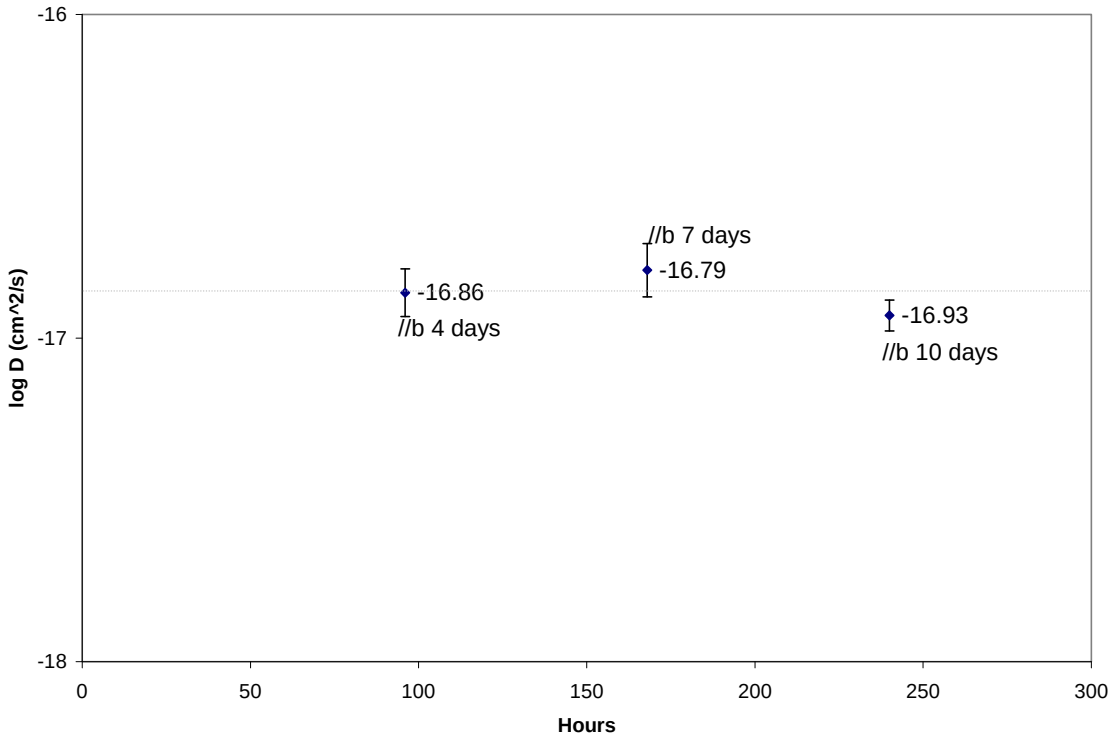

Figure 3.1: The above figure shows results of an experiment run at 1065 °C for 96, 168 and 240 hours. This time series analysis showed no systematic dependence of D(Nd) on time.

Diffusion coefficients and anisotropy:

Experiments were conducted over a range of temperatures from 1025-1150 °C at a constant oxygen fugacity to determine the diffusion coefficients as a function of temperature. Each run contained three samples, each prepared to allow diffusion to occur parallel to the a- b- and c- crystallographic axes, which corresponds to the three principal diffusion axes of orthopyroxene because of its orthorhombic crystallographic symmetry. The only exception was the run at 1065 °C. This run was the time series analysis and therefore contained three samples prepared for diffusion to occur parallel to the b-axis, and each sample was annealed for a different length of time. All samples have not yet been analyzed, but the results that have been obtained are presented in this work.

The diffusion coefficient is expressed as a function of temperature in the form of the Arrhenius equation $D=Do\ e^{(-E/RT)}$ where Do is a constant that incorporates the entropy of activation, E is the activation energy of diffusion, and R is gas constant. By experimentally finding the diffusion coefficient (D) at various temperatures and statistically regressing log (D) vs. 1/T, we can determine the activation energy and Do from the values for the slope and intercept, respectively (Fig. 3.2). Following this

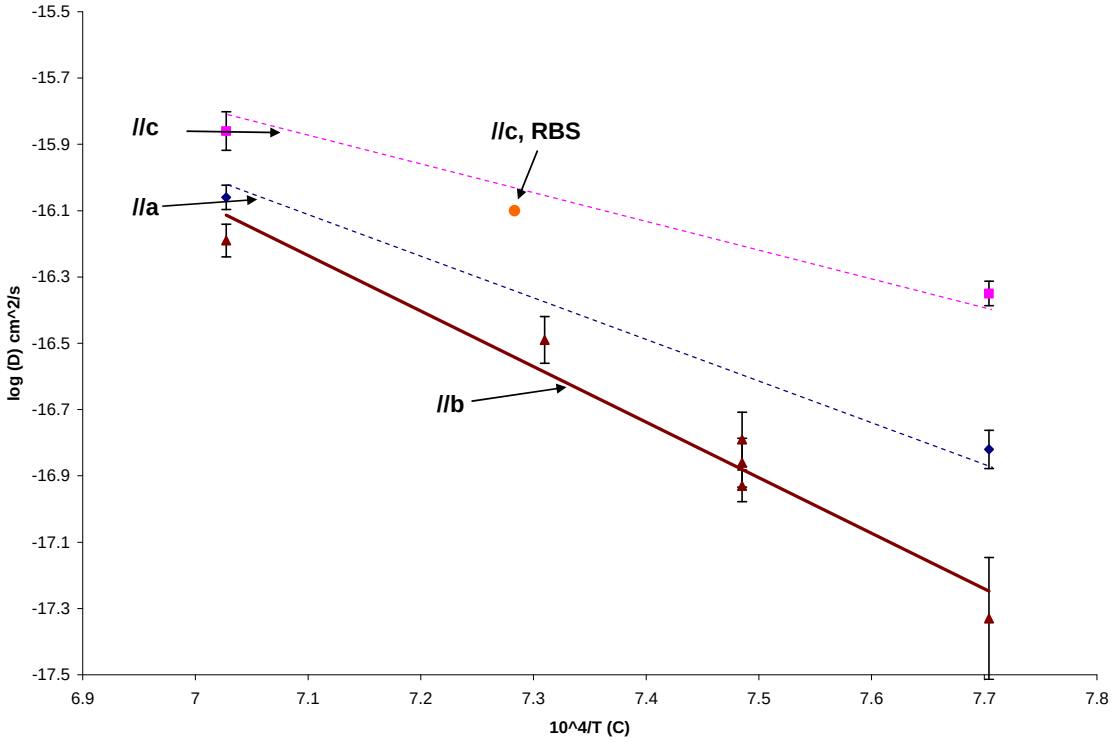

Figure 3.2: Arrhenius plot of Nd diffusion data for enstatite //b (dark red triangles), //a (blue circles) and //c (pink squares). Errors are calculated at 1 σ values. Experiments were run at 1 bar and WM-buffered conditions. The red circle is an experimental datum for Nd diffusion in enstatite //c at WM-buffered conditions analyzed by RBS from Ralf Dohmen. See text for details.

procedure, the diffusion coefficient for Nd in orthopyroxene parallel to the b-axis at $f(O_2)$ corresponding to that of the WM buffer was found to be:

$$D_{Nd} = 4.63(\pm .68)\ x10^{-5}e^{(-E/RT)}\ cm^2/s;\ E=321 \pm 41\ kJ/mol \qquad \text{Eq. 2}$$

where the errors are standard error.

The data illustrated in Fig. 3.2 show different rates of diffusion depending on the orientation of the crystal, and it appears that the difference is larger at lower temperatures. Neither of these findings is surprising, as orthopyroxene is an anisotropic mineral and diffusion is therefore expected to be anisotropic (Ganguly and Tazzoli, 1994). Our data show that for orthopyroxene $D_{Nd}(//c) > D_{Nd}(//a) > D_{Nd}(//b)$, with around a factor of 10 difference between the upper and lower limits at 1025 °C (Fig. 3.3). The observed diffusion anisotropy is in contrast to the conclusion reached by Charniak and Liang (2007) that there is no significant anisotropy for trivalent REE diffusion in orthopyroxene. Ganguly and Tazzoli (1974) predicted from structural considerations that diffusion of Fe and Mg in orthopyroxene should be fastest parallel to the c-axis and slowest parallel to the a-axis. Our data show a reverse relation for diffusion parallel to a and b axial directions.

We are awaiting analysis of several samples parallel to the a- and c-axes. Until those are obtained, we cannot acquire a meaningful least squares fit from the few experimental data points we have. We have obtained a well-constrained Arrhenius relation and activation energy along the b-axial direction. From the relative diffusion

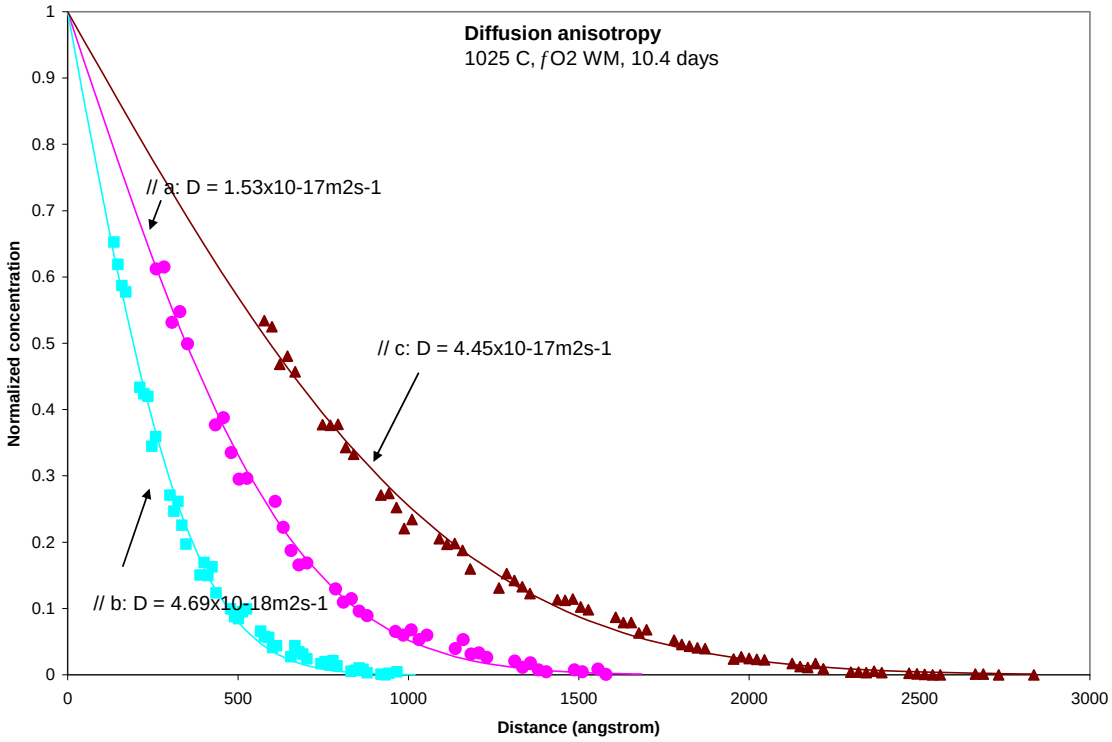

Figure 3.3: Diffusion anisotropy in orthopyroxene is slowest along the b direction (blue) and fastest along the c direction (brown) with the a direction (pink) intermediate between the two. There is a factor of 10 difference between the upper and lower limits at 1025 °C, as seen here.

rates from data at 1025 °C and 1150 °C, which show that D(//b)<D(//a)<D(//c), and assuming compensation behavior that states that there is a positive linear correlation between log Do and E, we conclude that E(//b) > E(//a) > E(//c). Using this constraint on the relative magnitudes of the activation energies, and knowing from previous diffusion studies that the activation energies among the different crystallographic directions will not change dramatically, we visually fit Arrhenius relations to the limited data for Nd diffusion parallel to a- and c-axial directions.

Calculating diffusion rate along an arbitrary axis:

When the rate of diffusion along the three orthogonal principal diffusion axes is known, the diffusion rate along any arbitrary axis can be calculated (e.g. Crank 1975). With the three data points at 1150 °C, the diffusion rate normal to the 210 plane was calculated to compare to the data presented by Cherniak and Liang.

In general a crystallographic symmetry axis defines the direction of a principal diffusion axis. Thus, the a, b and c crystallographic directions of orthopyroxene, which has an orthorhombic symmetry, define the directions of its principal diffusion axes. The 210 plane in orthopyroxene is a cleavage plane parallel to the c-axis (Fig. 3.4). It intersects the b-axis along the length of the unit cell and the a-axis at ½ the length of the unit cell. The axis normal to that plane intersects the c-axis at 90 degrees and the a- and b-axes at nearly 45 degrees. Exact angles are θ_1= 45.93°, θ_2= 44.07° and θ_3= 90°.

When the orientations of the three principal diffusion axes, ξ_1, ξ_2, and ξ_3, in an anisotropic medium are known, diffusion flux along any arbitrary direction, k, can be

easily calculated. If this arbitrary direction makes angles of θ_1, θ_2 and θ_3 with ξ_1, ξ_2, and ξ_3, respectively, then the flux is given by

$$J_K = -D_K \frac{\partial C}{\partial K} \qquad \text{Eq. 3}$$

where

$$D_K = D_{\xi i} \cos^2 \theta_{\xi i} + D_{\xi i} \cos^2 \theta_{\xi i} + D_{\xi i} \cos^2 \theta_{\xi i} \qquad \text{Eq. 4}$$

and $\partial C/\partial K$ is the concentration gradient along the direction K.

According to the above equation:

$$D_{\text{normal to (210)}} = D_a \cos^2 45.93° + D_b \cos^2 44.07° + D_c \cos^2 90° \qquad \text{Eq. 5}$$

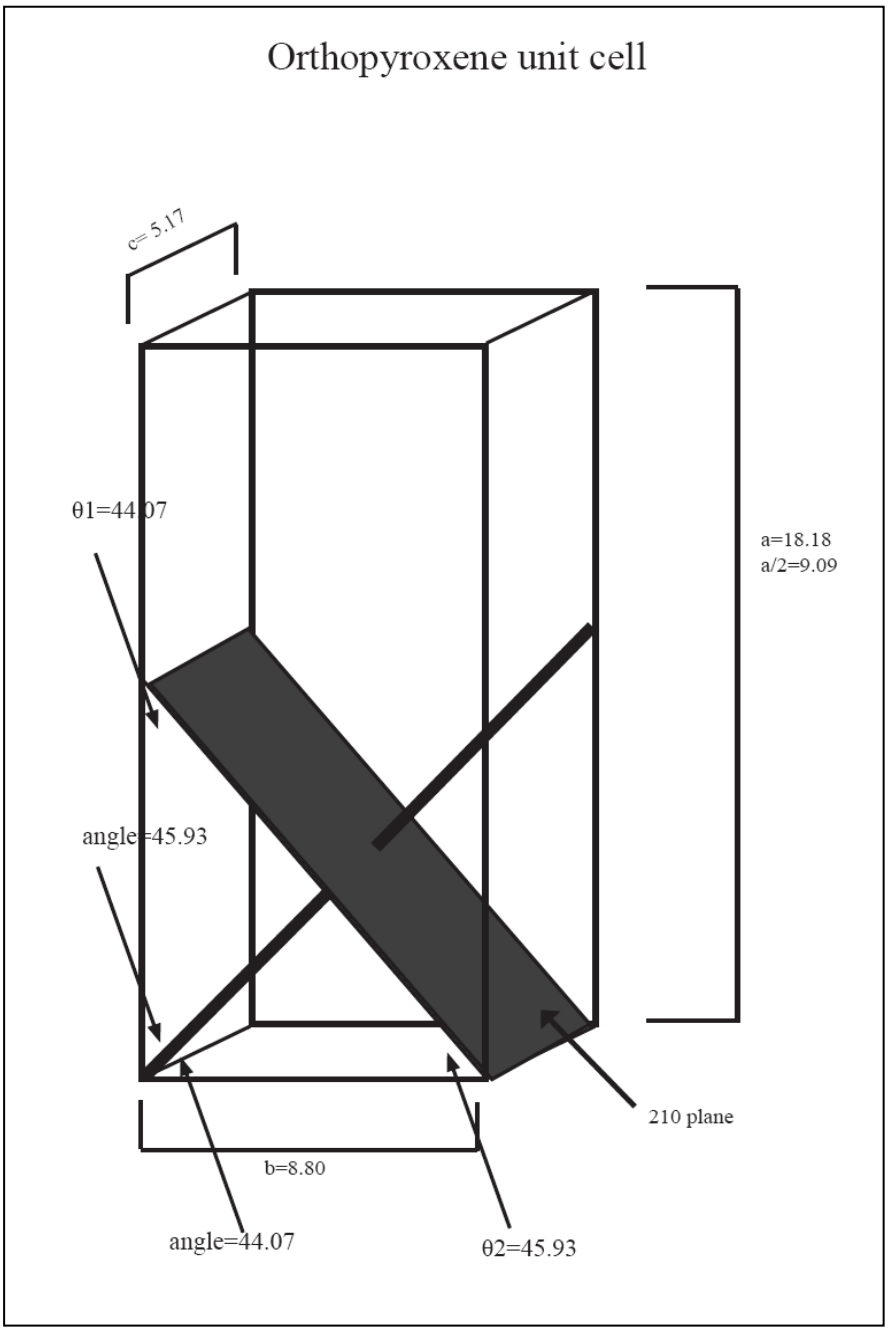

Figure 3.4: The 210 plane in orthopyroxene and angles with crystallographic axes. The axis normal to (210) intersects the c-axis at 90 degrees and the a- and b-axes at nearly 45 degrees. Exact angles are $\theta_1^{=}$ 45.93°, $\theta_2^{=}$ 44.07° and θ_3= 90°.

Comparison with other diffusion data:

There are few published experimental studies on REE diffusion in orthopyroxene. Cherniak and Liang (2007) reported results for REE in enstatite. Their experiments were conducted at 1 atm in air at a temperature range of 850-1250 °C with diffusion normal to (210). Cherniak and Liang suggested that there was no dependence of D for trivalent REE on ionic radius, oxygen fugacity or crystallographic orientation. Eu diffusion under iron-wüstite buffered conditions was found to be an order of magnitude faster than Eu diffusion in air, possibly because Eu is in the divalent state under IW buffered conditions (Cherniak and Liang, 2007).

Using Eq. 5 in the previous section, we calculated the diffusion normal to the 210 plane using the anisotropic diffusion data at 1 bar, 1150 °C, and $f(O_2)$ corresponding to WM buffer and found D(Nd) = 9.83E-18cm^2/s. The REE diffusion data presented by Cherniak and Liang (2007) overall is slower than those normal to the 210 plane calculated above from our anisotropic diffusion data at 1150 °C and our 1250 °C values are slower than those of Cherniak and Liang normal to the 210 plane (Fig. 3.5). However when a comparison of only their Nd data is made with the data from this study, it shows good agreement if one accepts the authors' statement that there is no diffusion dependence on $f(O_2)$. We extrapolated both D(REE) and D(Nd) in air //b to 827 C to compare diffusion rates with the rate published by Ganguly and Tirone (2001) (Fig. 3.5). While the diffusion rates presented in this work are somewhat faster than that of Cherniak and Liang, it is more than two orders of magnitude slower than that of Ganguly and Tirone.

An independent Nd diffusion in orthopyroxene experiment was conducted by Ralph Dohmen at Universität Bochum, Germany, to compare his result with those of our own. His experiment was conducted at 1100 °C, parallel to the c axis at WM-buffered conditions. Dohmen's experimental preparation included thin film deposition by laser evaporation of Nd_2O_3 and analysis by Rutherford backscattering (RBS), both methods which differ from those used in this study. However, as seen in Fig. 3.5, his results are in excellent agreement with our data parallel to the c axis. Schwandt et al. (1998) found Mg self-diffusion coefficients in orthopyroxene parallel to each of the three crystallographic axes. Because Nd is larger than Mg and has a higher valence charge, it would be expected to have a slower rate of diffusion in comparison to Mg. The diffusion rate of Nd presented in this study is more than two orders of magnitude slower than the rate of Mg presented by Schwandt et al. (Fig. 3.6).

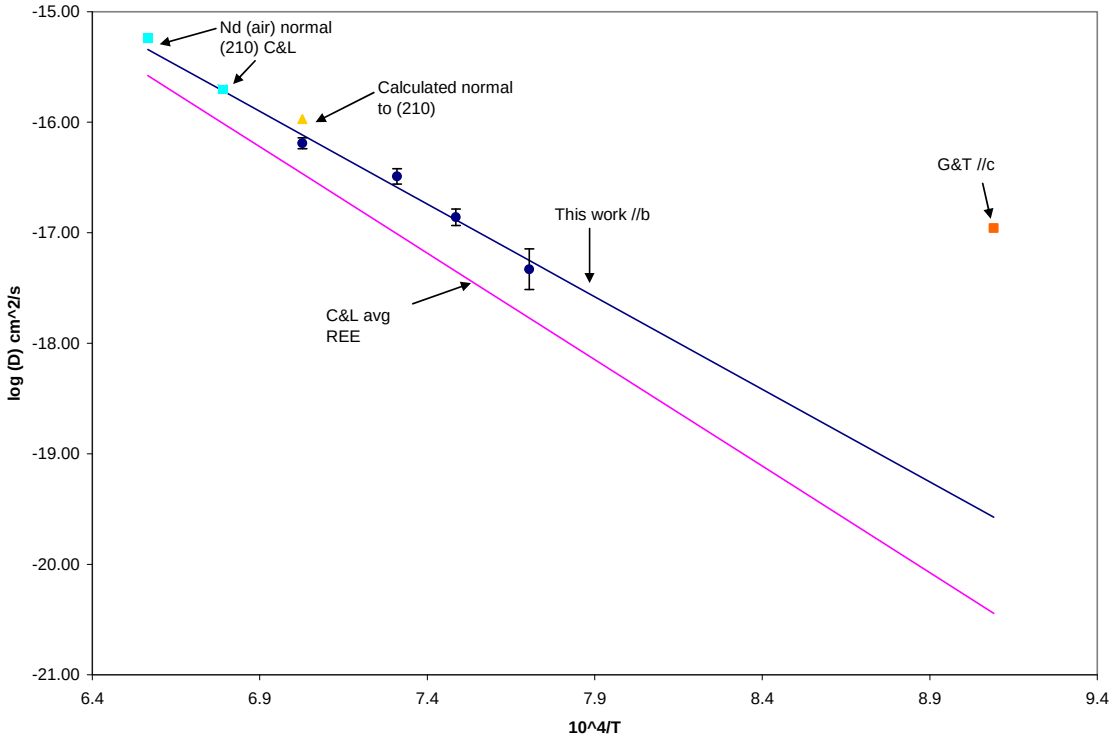

Figure 3.5: The calculated diffusion rate parallel to the axis normal to the 210 plane (orange triangle) is in good agreement with the diffusion rate found by Cherniak and Liang for the same crystallographic direction (blue squares) under different fugacity conditions. The overall REE diffusion rates (pink line) is slower than that of the Nd diffusion rate alone and slower than the Nd diffusion rates presented in this work. The Nd diffusion datum presented by Ganguly and Tirone (red square) is faster than others discussed in this study.

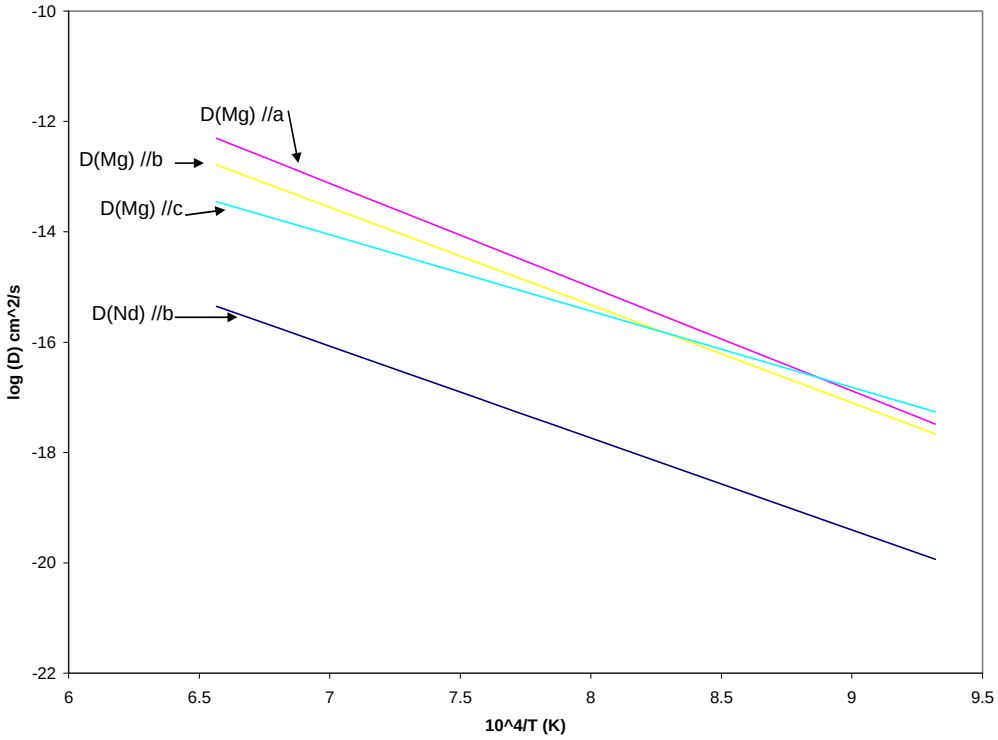

Figure 3.6: The diffusion rate of Nd presented in this study (blue line, above) is more than two orders of magnitude slower than the rate of Mg presented by Schwandt et al. (1998). This difference in diffusion rate is expected because Nd is larger than Mg and has a higher valence charge.

Chapter 4. Applications

Closure temperature and Sm-Nd age of orthopyroxenes:

^{147}Sm decays to ^{143}Nd by the emission of α particles, and has a half-life ($t_{1/2}$) of 106.0×10^9 years. This decay system has been widely used for dating rocks and minerals in both terrestrial and planetary samples. The interpretation of Sm-Nd and, in general, of any mineral age depends critically on the temperature at which the daughter products become isolated within the minerals of interest. In a system experiencing monotonic cooling, this temperature is known as the closure temperature, T_c. In a given rock sample, different decay systems often yield different ages as a result of different extents of loss of daughter products from the minerals during cooling. This property has led to the use of T_c vs. age diagrams in which the Tc-age combinations of different decay systems in a given rock sample or terrain are plotted and fitted to obtain cooling rates. An example of this is the diagram below (Fig. 4.1 from Spear and Parish, 1996) in which a plot of temperature vs. time is shown for the Valhalla Complex, British Columbia, Canada.

The concept of closure temperature was first formalized by Dodson (1973). He showed that the mineralogical closure temperature of a specific decay system depends on cooling rate, grain size of the mineral, its shape and its diffusion kinetic properties. Dodson (1973) derived the following expression that allows one to calculate T_c as a function of cooling rate and grain size, if the diffusion parameters are known.

$$\frac{E}{RT_c} = \ln\left(\frac{-ART_c^{\,2}D_o}{E\left(dT/dt\right)_{T_c}a^2}\right) \qquad \text{Eq. 6}$$

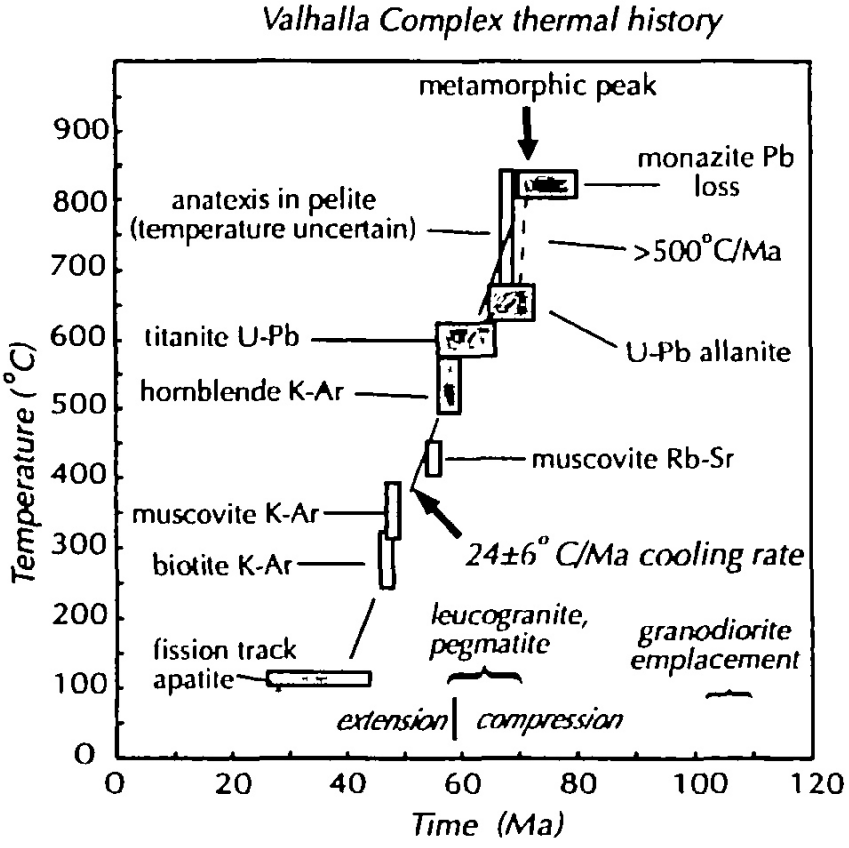

Fig. 4.1: Temperature vs. time plot showing a cooling rate for the Valhalla Complex from Spear and Parrish, 1996.

Here D_o and E are the pre-exponential factor and activation energy in the Arrhenius expression of the diffusion coefficient ($D = D_o\exp(-E/RT)$), $(dT/dt)_{@Tc}$ is the cooling rate at T_c, A is a geometric factor that is given by $A = e^G$ (G is 4.0066 for sphere, 3.29506 for cylinder and 2.15821 for plane sheet), and *a* is a characteristic dimension (radius for sphere and cylinder, and half-width for plane sheet) of the effective diffusion domain.

Dodson (1973) assumed an asymptotic cooling model that is given by

$$\frac{1}{T} = \frac{1}{T_o} + \eta t \qquad \text{Eq. 7}$$

where T_o is the initial temperature at the onset of cooling, and η is a cooling time constant with dimension of $K^{-1}t^{-1}$. Since $dT/dt = -\eta T^2$, the classic Dodson (1973) equation can be expressed in terms of η as

$$\frac{E}{RT_c} = \ln\left(\frac{ARD_o}{E\eta a^2}\right) \qquad \text{Eq. 8}$$

There are two important assumptions behind the derivation of the Dodson expression for T_c. He assumed that the matrix of the target mineral behaves as a homogeneous infinite reservoir (which is possible only if the matrix has a large mass and very large diffusion coefficient relative to that of the target mineral), and (b) there is

sufficient diffusive loss from the mineral such that the initial composition is not preserved even at the core of a grain. The latter assumption makes the T_c independent of the initial temperature, T_o. However, this assumption of complete "memory loss" is not usually valid for minerals such as garnet and pyroxene that are characterized by slow diffusion properties. Ganguly and Tirone (1999) addressed the problem of the effect of T_o on T_c, and derived a more general analytical expression of T_c that is formally the same as Dodson's equation if the term A is replaced by A′ where $A' = e^{G+g}$, with g being a function of the grain geometry and a dimensionless variable M that is given by

$$M = \frac{-RD_{T_o}T^2}{E\left(dT/dt\right)_T a^2} = \frac{RD_{T_o}}{E\eta a^2} \qquad \text{Eq. 9}$$

Analytical expressions for g and tables of g values for different geometries are given by Ganguly and Tirone (1999) and Ganguly and Tirone (2001), respectively. Closure temperature for the Sm-Nd decay system in orthopyroxene, as calculated from the modification of Dodson's equation by Ganguly and Tirone (1999), is illustrated in Fig. 4.2 as a function of cooling rate at T_c, T_o and grain size for plane sheet and spherical geometry, using D_{Nd}(//b), as determined in this study.

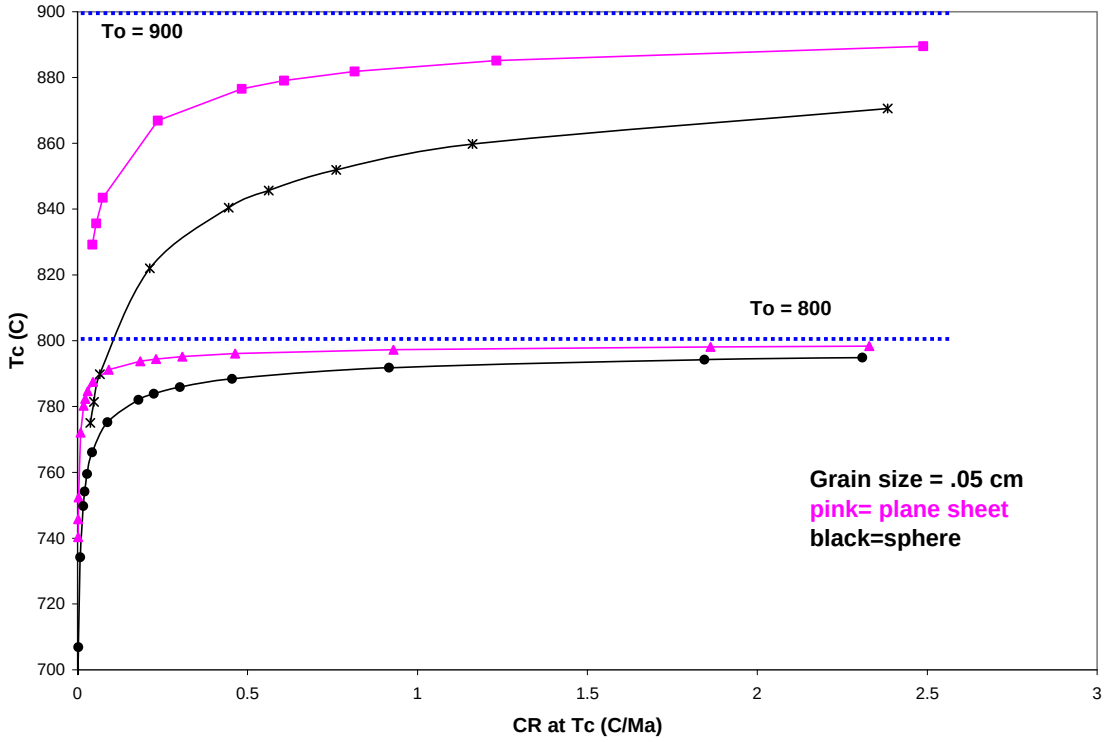

Figure 4.2: Closure temperature (Tc) of Nd in orthopyroxene as a function of initial temperature (To), grain size and cooling rate for plane sheet and spherical geometries according to the formulation of Ganguly and Tirone (1999) and software developed by these authors. This formulation is a modification of the Dodson formulation (Dodson, 1973). The modification allows for slowly diffusing species in which the mineral's composition may not completely homogenize at To, and therefore treats Tc as a function of To. D(Nd) //b from this work was used for closure temperature calculations.

From the above discussion and Fig. 4.2, it is evident that a specific decay system does not have a unique T_c in a given mineral but that the T_c varies as a function of grain size and cooling rate; in addition it is also affected by T_o when the diffusive loss is not sufficient to completely erase the "memory" of the initial condition from the mineral grains. Thus, the common practice of using a T_c vs. age diagram to determine cooling rate is circular because it depends on closure temperature, which itself depends on cooling rate. It is less problematic if the T_c values of the specific decay systems can be further restricted after allowing for the effects of the usual range of grain size, cooling rate and T_o in the natural environments. If the grain size and T_o are known in a specific situation, then one may be able to compute a restricted range of T_c for certain decay systems allowing for reasonable variation of cooling rate that may be inferred from the nature of rock type and terrain (e.g. ~5 – 30 ^oC/Myr for regionally metamorphosed rocks), and thus construct a T_c vs. age diagram using multiple decay systems and further refine the cooling rate from the best fit to all the data.

Ganguly et al. (1998) and Ganguly and Tirone (1999, 2001) developed an alternative approach to the retrieval of cooling rate that completely avoids the tautological problem associated with the common approach to the retrieval of cooling rate from T_c vs. age relations. The formulation requires only knowledge of the grain size and the extent of resetting – or age loss – of mineral age, according to a specific decay system, during cooling. The relationship governing the resetting of age to cooling rate is given by the following equation (parameters are explained above):

$$\Delta t = \frac{R}{\eta E}\left[\ln M + G + g\right] \qquad \text{Eq. 10}$$

Ganguly and co-workers (Ganguly et al. 1998; Ito and Ganguly, 2005, Ganguly et al. 2007) and others have applied this relation to retrieve cooling rates from knowledge of resetting of mineral ages for specific decay systems (e.g. resetting of Sm-Nd age of garnet in granulites and of ^{53}Mn-^{53}Cr ages of olivine and pyroxenes in meteorites). Here we discuss one application of the above relation to a controversial topic of Sm-Nd mineral age of a stony-iron meteorite, namely the Morristown mesosiderite.

Prinzhofer et al. (1992) found that the Sm-Nd internal isochron defined by plagioclase, phosphates and orthopyroxene of the Morristown mesosiderite yielded an age of 4470 ± 20 Ma, which is ~ 90 Ma younger than the U-Pb age of 4560 ± 31 Ma for the Estherville mesosiderite, as determined by Brouxel and Tatsumoto (1991). Prinzhofer et al. (1992) explained this age difference by an 'impulsive' disturbance model in which the Sm-Nd isotopic composition of plagioclase, which had the lowest REE concentration, was disturbed by a short duration metamorphic event after the system had closed in all minerals. It was assumed that the Sm-Nd concentrations of orthopyroxene were not affected because, according to data by Sneeringer et al. (1984), Sm diffusion in clinopyroxene is very slow, and diffusion kinetics in orthopyroxene, therefore, probably behaved similarly. The model also assumed that the compositions of the phosphates, which exchanged REE with plagioclase, were not affected, as these were the main hosts of Sm and Nd because of their larger mass abundance. This 'impulsive' disturbance of

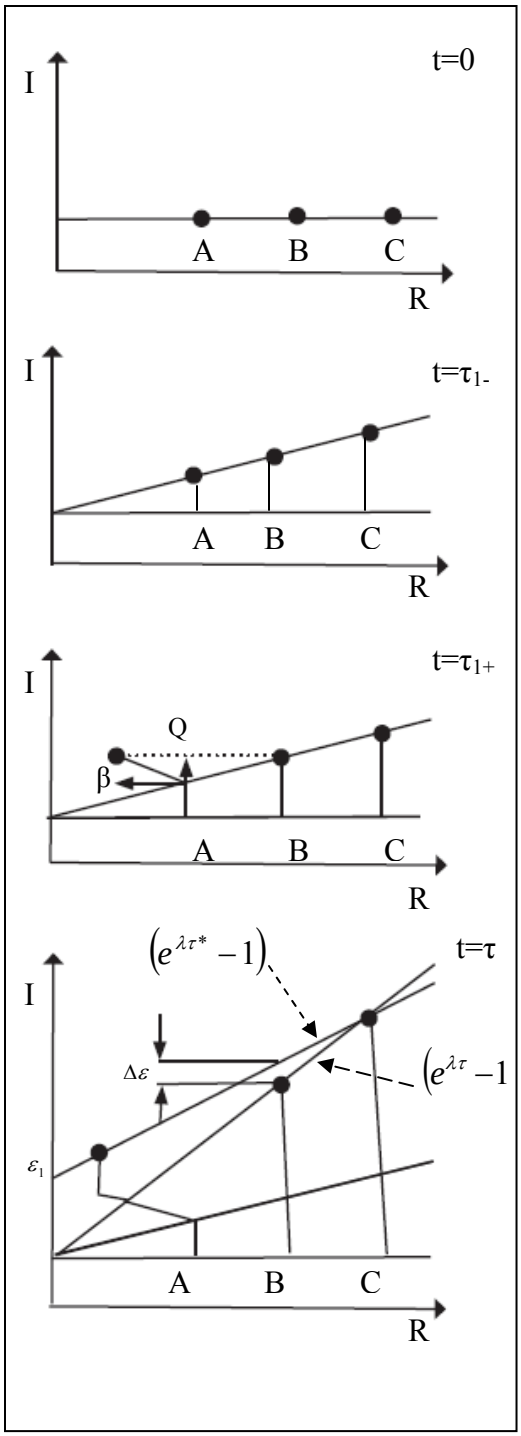

Fig. 4.3: Sm-Nd internal isochron demonstrating 'impulsive' disturbance model for mesosiderites as proposed by Prinzhofer et al. 1992 (recreated).

REE concentration in plagioclase would, therefore, create an apparent Sm-Nd mineral isochron defined by plagioclase, phosphate and pyroxene (in order of increasing Sm/Nd ratio) with a lower slope than that without the disturbance, thus giving the appearance of a younger age (Fig. 4.3 from Prinzhofer et al, 1992).

Stewart et al. (1994) addressed the Sm-Nd chronology of mesosiderites, and determined that such an 'impulsive' disturbance of the decay system in pyroxene and plagioclase might occur by cooling under metal or regolith blankets. To quantify this, the authors inferred the Sm-Nd diffusion data in plagioclase and made the same assumption as did Prinzhofer et al. (1992) regarding the Sm-Nd diffusion in orthopyroxene. Their conclusion was that in order to escape significant resetting of the Sm-Nd system during cooling, the mesosiderite clasts must have been buried no deeper than 10-20 m in metal or 1 m in regolith.

The 'impulsive' disturbance model of Prinzhofer et al. (1992) was contested by Ganguly and Tirone (2001), who suggested that the resetting of ~ 90 Ma for Sm-Nd age is expected if one accepts the slow cooling rate of mesosiderites commencing from 727^{o}C ($\eta = 1.8 \times 10^{-12}$ $K^{-1}y^{-1}$ corresponding to cooling rate of 0.5^{o}C/Myr at 250^{o}C) that was calculated by Ganguly et al. (1996) from the Fe^{2+}-Mg ordering data of orthopyroxenes. In arriving at this conclusion, Ganguly and Tirone (2001) used their preliminary Nd diffusion datum in orthopyroxene (Fig. 3.4) and assumed, by analogy with the diffusion kinetic behavior of garnet, that the activation energy of Nd diffusion in orthopyroxene is similar to that of its Fe-Mg interdiffusion, which is ~ 250 kJ/mol.

Here we revisit the problem of the resetting of Sm-Nd age of the Morristown orthopyroxene by using the Nd diffusion data determined in this study. For this purpose, we use the Arrhenius parameters for D_{Nd}(//b), and allow for a factor of 10 enhancement of the bulk diffusivity of Nd diffusion in orthopyroxene relative to that in the b direction, on the basis of the preliminary anisotropic diffusion data shown in Fig. 3.2. The average grain size of orthopyroxene crystals in the Morristown mesosiderites is ~ 50 μm. These data yield M = 0.08 and g values of 1.005 and 0.195 for plane sheet and spherical geometries, respectively. Substitution of the inferred M and g values along with the η value from Ganguly et al. (1996) and the 10 x D_{Nd} calculated at T_o = 1000 K from the Nd diffusion obtained in this study (= 7.96 x10^{-21} cm^2/s)D_{Nd}(//b) in Eq. (11) yields resetting Δt ~ 13 and 32 Myr for plane sheet and spherical geometries, respectively, during cooling. Thus, the observed ~ 90 resetting of the Sm-Nd age of Morristown orthopyroxene in the Morristown mesosiderite could not have been solely due to slow cooling. An "impulsive heating" or some other process is needed to explain the resetting of the Sm-Nd age.

Cooling rates and REE element zoning in orthopyroxenes:

When partition coefficients are known for a given elements in a given pair of minerals, much can be determined about the thermal history and interaction of these minerals at equilibrium. However, only a portion of the entire mineral will achieve equilibrium. Generally, it can be assumed that equilibrium is achieved at the mineral-mineral interface, but how far that equilibrium is achieved toward the core of the mineral depends on several factors, namely initial temperature, cooling rate, grain size and the

rate of diffusion. Because of this, if one knows the grain size, diffusion rate and initial temperature, the observed concentration profiles can be used to determine cooling rates of a mineral pair and conversely, given a particular cooling rate, specific concentration profiles can be projected.

Cherniak and Liang (2007) used REE diffusion rates in diopside found by Van Orman et al. (2001, 2002a) and their own average REE diffusion rates discussed throughout this paper to examine zoning profiles that would occur in a one-dimensional opx-cpx pair in spinel peridotite under a continuous cooling regime. The system was modeled to begin at 1400 °C and to cool 1000 °C at a constant rate of 20 °C/Ma. They found in their simulations that while only a small near interface segment of clinopyroxene is affected by diffusion, a much greater distance from the interface in the orthopyroxene is affected by diffusion, thus making the diffusion induced compositional zoning in orthopyroxene an important observational property for the retrieval of cooling rate of natural samples. This is a consequence of strong interfacial fractionation of REE and relatively much faster diffusion in orthopyroxene compared to clinopyroxene (Van Orman, 2002). The variations along the rim were due to increasing REE^{3+} cpx-opx equilibrium partition coefficients with decreasing temperature while the essentially unaffected cores were due to slow diffusion rates. Cherniak and Liang concluded that high REE^{3+} abundances in unequilibrated cores of large orthopyroxene crystals are likely preserved due to relatively slow diffusion and could be used to learn more about the thermal history of spinel peridotite. While their model is correct, the time inferences and profiles determined from their slower diffusion rate are different from what we calculated

with the diffusion rate presented in this work. In order to illustrate this problem of inference of cooling rate of spinel-peridotite on the basis of REE zoning in orthopyroxene, we recalculated the profiles with the new Nd diffusion data.

We kept the clinopyroxene diffusion rates and all partition coefficients the same and assumed equilibrium was maintained at the interface and zero flux at core of the mineral. The profiles were adjusted simply by considering the proportionality of the diffusion profile to the square root of the product of the diffusion rate and time:

$$X \propto \sqrt{Dt}$$

To compare the profile resulting from the diffusion rate of this study (TS) to that of Cherniak and Liang (CL) we look at the ratio:

$$\frac{X_{CL}}{X_{TS}} = \frac{\sqrt{D_{CL}t}}{\sqrt{D_{TS}t}}$$

therefore

$$X_{TS} = X_{CL}\sqrt{\frac{D_{TS}}{D_{CL}}}$$

Cherniak and Liang used an average diffusion rate for REE^{3+} in orthopyroxene assuming no anisotropy or dependence on oxygen fugacity of

$$D_{REE}^{3+} = 1.2\text{x}10^{-3} \exp(-369{,}000/RT)$$

Whereas the diffusion rate found in this study for Nd^{3+} in orthopyroxene //b at WM buffer was

$$D_{Nd}^{3+} = 4.6x10^{-5} \exp(-320{,}925/RT)$$

The dotted line in Fig. 4.4 represents the concentration profile that would develop at t=20 Ma with D_{TS} compared to D_{CL} represented by the solid line. Given the fact that D_{TS} is approximately three times faster than D_{CL}, the solid line represents what would be the equivalent of approximately t=6.5 Ma for a diffusion rate of D_{TS}.

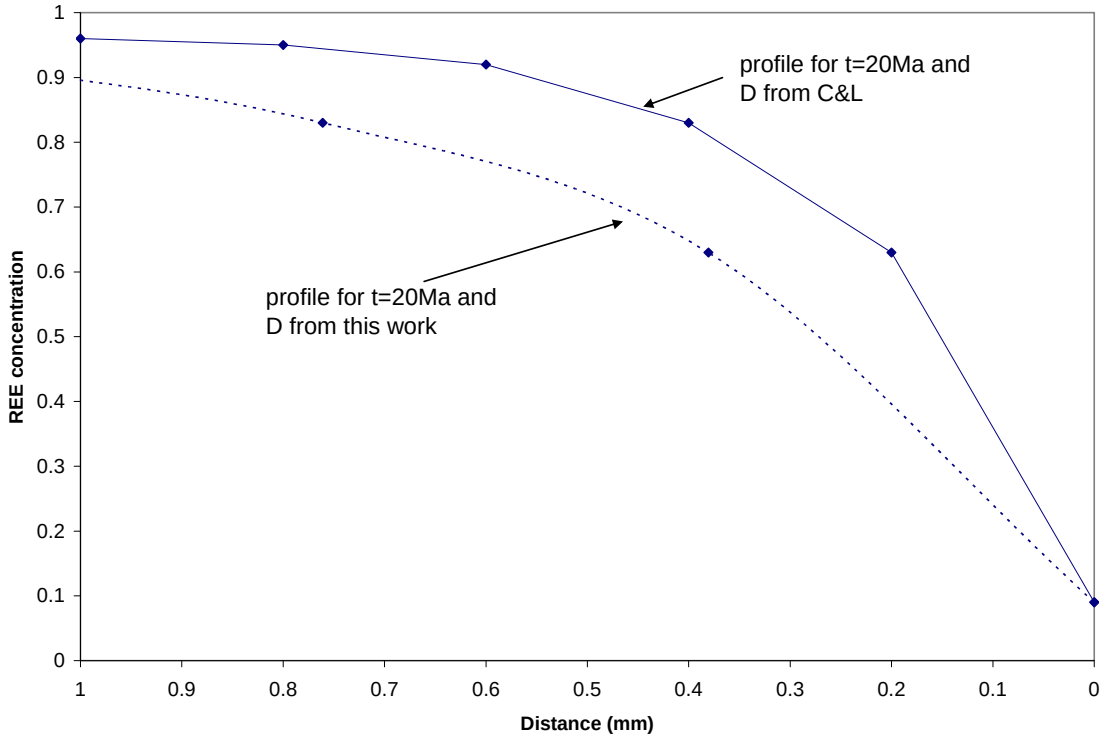

Figure 4.4: The concentration profile that would develop at t=20 Ma with a diffusion rate of Nd in orthopyroxene found in this study (dotted line) compared to t=20 Ma calculated with the diffusion rate of Cherniak and Liang (solid line). Given that the diffusion rate presented in this study is approximately three times faster than D_{CL}, the solid line represents what would be the equivalent of approximately t=6.5 Ma for the diffusion rate presented here.

Chapter 5. Conclusions and future work

We determined the Arrhenius equation for neodymium (Nd) diffusion in orthopyroxene parallel to the b- axial direction as a function of temperature at 1 bar pressure and at $f(O_2)$ corresponding to that of the wüstite-magnetite buffer to be $D_{Nd} = 4.63x10^{-5}e^{(-E/RT)}$ cm^2/s; E=321 kJ/mol. In addition, we developed an approximate idea of the extent of diffusion anisotropy of Nd in orthopyroxene, in which the three crystallographic axes define the directions of the three principal diffusion axes. It was found that D(//c) > D(//a) > D(//b) with up to a factor of 10 change of diffusivity between D(//c) and D(//b), and that the difference between the diffusivities parallel to b and a axes is relatively small. From these data, we calculated Nd diffusion normal to the (210) plane of orthopyroxene in order compare our data with those of Cherniak and Liang (2007), who determined REE^{3+} diffusion in orthopyroxene in the same direction. We found that our Nd diffusion data normal to 210 plane at 1 bar, 1150 °C was a factor of three greater than what follows from the Arrhenius relation given by Cherniak and Liang for REE^{3+} diffusion in orthopyroxene, but is in good agreement with their specific experimental data for Nd diffusion if one accepts their argument there is no dependence on oxygen fugacity. However, this brings into question, their conclusion that trivalent REE diffusion in orthopyroxene is essentially independent of the nature or radius of the REE.

After comparing the diffusion data presented in this study with previously published data, we used our diffusion data parallel to the b-axis to calculate the closure temperature of Sm-Nd decay system in orthopyroxene grains of plane sheet habit

spherical habit as a function of initial temperature, cooling rate and grain size, showing that initial temperature significantly impacts closure temperature for slowly diffusing species. The Nd diffusion data were also used to interpret the resetting of mineral age defined by an internal isochron involving orthopyroxene in the Morristown mesosiderite, concluding that some 'impulsive' disturbance or other event would be required for the observed amount of age loss. The data was also used to show the problem of inference of cooling rate of spinel-peridotite on the basis of REE zoning in orthopyroxene.

There are still many unanswered questions, such as how much of an effect oxygen fugacity or ionic radius has on diffusion rate, or how much diffusion anisotropy there is for Nd in orthopyroxene. In order to better understand these issues we will continue experiments for this study. Specifically for this work, we will anneal two samples //b, at 1095 °C for 98.5 hours, one at WM+1.5 and one at WM -2 to determine the effect of fugacity. We will also analyze several samples that have already been annealed to better constrain the c and a diffusion rates and get Arrhenius relations. We are currently waiting for results of analyses of samples //a //b and //c at 975 °C, and //a and //c at 1095 °C.

References

Buening, D. K., and Peter R. Buseck. "Fe-mg Lattice Diffusion in Olivine." Journal of Geophysical Research 78.29 (1973): 6852-62.

Chakraborty, S., et al. "Mg Tracer Diffusion in Synthetic Forsterite and San Carlos Olivine as a Function of P, T and fO2." Physics & Chemistry of Minerals 21.8 (1994): 489-500.

Cherniak, DanieleJ, and Yan Liang. "Rare Earth Element Diffusion in Natural Enstatite." Geochimica et Cosmochimica Acta 71.5 (2007): 1324-40.

Crank, J. The Mathematics of Diffusion. 2nd ed. ed. Oxford: Oxford University Press, 1975.

Dodson, M. H. "Closure Temperature in Cooling Geochronological and Petrological Systems." Contributions to Mineralogy and Petrology 40 (1973): 259-64.

Ganguly, J., and V. Tazzoli. "Fe2+-mg Interdiffusion in Orthopyroxene: Retrieval from the Data on Intracrystalline Exchange Reaction." American Mineralogist 79.9-10 (1994): 930-7.

Ganguly, J., M. Tirone, and R. L. Hervig. "Diffusion Kinetics of Samarium and Neodymium in Garnet, and a Method for Determining Cooling Rates of Rocks." Science 281.5378 (1998): 805-7.

Ganguly, J. "Diffusion Kinetics in Minerals: Principles and Applications to Tectono-Metamorphic Processes." European Mineralogical Union, Notes in Mineralogy 4 (2003): 271--309.

Ganguly, Jibamitra, Motoo Ito, and Xiaoyu Zhang. "Cr Diffusion in Orthopyroxene: Experimental Determination, 53Mn–53Cr Thermochronology, and Planetary Applications." Geochimica et Cosmochimica Acta, 71.15 (2007): 3915-25.

Ganguly, Jibamitra, Hexiong Yang, and Subrata Ghose. "Thermal History of Mesosiderites: Quantitative Constraints from Compositional Zoning and Fe-mg Ordering in Orthopyroxenes." Geochimica et Cosmochimica Acta 58.12 (1994): 2711-23.

Griffin, W. L., et al. "Trace-Element Zoning in Mantle Minerals: Metasomatism and Thermal Events in the Upper Mantle." Canadian Mineralogist 34.6 (1996): 1179-93.

Ito, M., and J. Ganguly. "Diffusion Kinetics of Cr in Olivine and 53Mn-53Cr Thermochronology of Early Solar System Objects." Geochimica et Cosmochimica Acta 70.3 (2006): 799-809.

---. "Potassium Diffusion in Melilite: Experimental Studies and Constraints on the Thermal History and Size of Planetesimals Hosting CAIs." Meteoritics and Planetary Science 39.12 (2004): 1911-9.

Lasaga, A. C. Kinetic Theory in the Earth Sciences. Princeton, New Jersey:, 1998.

Misener, D. J. "Cationic Diffusion in Olivine to 1400 Degrees C and 35 Kbar." Carnegie Institution of Washington. Washington 634 (1974): 117-29.

Prinzhofer, A., D. A. Papanastassiou, and G. J. Wasserburg. "Samarium-Neodymium Evolution of Meteorites." Geochimica et Cosmochimica Acta 56.2 (1992): 797-815.

Schwandt, C. S., R. T. Cygan, and H. R. Westrich. "Magnesium Self-Diffusion in Orthoenstatite." Contributions to Mineralogy and Petrology 130.3-4 (1998): 390-6.

Sneeringer, M., S. R. Hart, and N. Shimizu. "Strontium and Samarium Diffusion in Diopside." Geochimica et Cosmochimica Acta 48.8 (1984): 1589-608.

Spear, F. S., and R. R. Parrish. "Petrology and Cooling Rates of the Valhalla Complex, British Columbia, Canada." Journal of Petrology 37.4 (1996): 733-65.

Stewart, B. W., D. A. Papanastassiou, and G. J. Wasserburg. "Sm-Nd Chronology and Petrogenesis of Mesosiderites." Geochimica et Cosmochimica Acta 58.16 (1994): 3487-509.

Tirone, Massimiliano, et al. "Rare Earth Diffusion Kinetics in Garnet: Experimental Studies and Applications." Geochimica et Cosmochimica Acta, 69.9 (2005): 2385-98.

Van Orman, J. A., T. L. Grove, and N. Shimizu. "Diffusive Fractionation of Trace Elements during Production and Transport of Melt in Earth's Upper Mantle." Earth and Planetary Science Letters 198.1-2 (2002): 93-112.

Van Orman, J. A., and T. L. Grove. "Rare Earth Element Diffusion in Diopside: Influence of Temperature, Pressure, and Ionic Radius, and an Elastic Model for Diffusion in Silicates." Contributions to Mineralogy and Petrology 141.6 (2001): 687-703.

Witt-Eickschen, G., and H. St C. O'Neill. "The Effect of Temperature on the Equilibrium Distribution of Trace Elements between Clinopyroxene, Orthopyroxene, Olivine and Spinel in Upper Mantle Peridotite." Chemical Geology 221.1-2 (2005): 65-101.